# Influence of Spatial Dipole Pattern in Asian Aerosol Changes on East Asian Summer Monsoon

CHAO LIU,[a] YANG YANG,[a] HAILONG WANG,[b] LILI REN,[a] JIANGFENG WEI,[c] PINYA WANG,[a] AND HONG LIAO[a]

[a] *Jiangsu Key Laboratory of Atmospheric Environment Monitoring and Pollution Control, Jiangsu Collaborative Innovation Center of Atmospheric Environment and Equipment Technology, School of Environmental Science and Engineering, Nanjing University of Information Science and Technology, Nanjing, Jiangsu, China*

[b] *Atmospheric Sciences and Global Change Division, Pacific Northwest National Laboratory, Richland, Washington*

[c] *School of Atmospheric Sciences, Nanjing University of Information Science and Technology, Nanjing, Jiangsu, China*

(Manuscript received 10 May 2022, in final form 13 October 2022)

ABSTRACT: Since China implemented the Air Pollution Prevention and Control Action Plan in 2013, the aerosol emissions in East Asia have been greatly reduced, while emissions in South Asia have continued to increase. This has led to a dipole pattern of aerosol emissions between South Asia and East Asia. Here, the East Asian summer monsoon (EASM) responses to the dipole changes in aerosol emissions during 2013–17 are investigated using the atmosphere model of Community Earth System Model version 2 (CESM2). We show that decreases in East Asian emissions alone lead to a positive aerosol effective radiative forcing (ERF) of 1.59 (±0.97) W $m^{-2}$ over central-eastern China (25°–40°N, 105°–122.5°E), along with a 0.09 (±0.07)°C warming in summer during 2013–17. The warming intensified the land–sea thermal contrast and increased the rainfall by 0.32 (±0.16) mm $day^{-1}$. When considering both the emission reductions in East Asia and increases in South Asia, the ERF is increased to 3.39 (±0.89) W $m^{-2}$, along with an enhanced warming of 0.20 (±0.08)°C over central-eastern China, while the rainfall insignificant decreased by 0.07 (±0.16) mm $day^{-1}$. It is due to the westward shift of the strengthened western Pacific subtropical high, linked to the increase in black carbon in South Asia. Based on multiple EASM indices, the reductions in aerosol emissions from East Asia alone increased the EASM strength by almost 5%. Considering the effect of the westward shift of WPSH, the dipole changes in emissions together increased the EASM by 5%–15% during 2013–17, revealing an important role of South Asian aerosols in changing the East Asian climate.

KEYWORDS: Monsoons; Climate models; Aerosol radiative effect; Aerosols/particulates

## 1. Introduction

Anthropogenic emissions of aerosols and their precursors have increased significantly since the preindustrial era, especially in East Asia and South Asia due to industrialization and urbanization (Zhang et al. 2012). As a result of the increase in emissions, particle pollution has been a big concern over these regions. To mitigate the air pollution, the Chinese government issued and implemented the air pollution prevention and control action plan in 2013 and consequently the anthropogenic aerosol (AA) emissions have been greatly reduced in East Asia (Zheng et al. 2018). Meanwhile, AA emissions in South Asia are continually increasing, which leads to a spatial dipole pattern of AA emission changes over the broad continental region of South and East Asia (as shown in Fig. S1 in the online supplemental material; Samset et al. 2019; Ramachandran et al. 2022).

Aerosols are the main pollutant of concern due to their adverse effects on atmospheric visibility and human health (Bell and Davis 2001; Cohen et al. 2017). Besides their environmental impacts, aerosols can also influence the regional and global climate by changing the atmospheric radiation budget via scattering and absorbing solar radiation and modifying cloud microphysical properties (Yu et al. 2013; Yang et al. 2017a,b, 2019, 2020, 2022).

The East Asian summer monsoon (EASM) is a crucial component of the Asian atmospheric circulation and climate system, driven by the temperature difference between the Asian continent and its surrounding oceans (Ding and Chan 2005). EASM provides 40%–50% of the annual total precipitation for southern China, and 60%–70% for northern China (Lei et al. 2011). Changes in EASM can have a significant impact on local infrastructure, agriculture, water resources and global water cycle (Ding and Chan 2005).

Many previous studies have illustrated the important role that AA has played in changing EASM (Lau et al. 2008; Li et al. 2016). Zhang et al. (2011) used the atmospheric general circulation model of the Beijing Climate Center (BCC_AGCM) with prescribed sea surface temperature (SST) and sea ice concentration (SIC) to study the response of EASM to the direct radiative effects of AA. They reported that increases in aerosols would cause anomalous northerlies, reduce the northward moisture transport, and weaken the EASM precipitation in eastern and southern China between 15° and 30°N. Using the National Center for Atmospheric Research (NCAR) Community Atmospheric Model version 5 (CAM5) driven by prescribed SST and SIC with aerosol direct, semidirect and indirect effects considered, Jiang et al. (2013) investigated the AA impact on the EASM between 1850 and 2000.

Supplemental information related to this paper is available at the Journals Online website: https://doi.org/10.1175/JCLI-D-22-0335.s1.

*Corresponding author*: Yang Yang, yang.yang@nuist.edu.cn

DOI: 10.1175/JCLI-D-22-0335.1

They concluded that the increased AA reduced the land–sea thermal contrast, reduced precipitation in North China, and increased precipitation in South China and its adjacent oceans, primarily attributed to the effects of sulfate and primary organic matter (POM) aerosols. Xie et al. (2016) also indicated that the effects of AA on the monsoonal circulation and precipitation were stronger in weak monsoon years than in strong monsoon years based on CAM5 simulations. Using a coupled atmosphere–ocean–mixed-layer model, Tian et al. (2018) and Dong et al. (2019) found that the increase in AA led to anomalous moisture flux divergence and decreased precipitation over northern China, which weakened the EASM during the recent decades. Mu and Wang (2020) used simulations from 16 Coupled Model Intercomparison Project Phase 5 (CMIP5) models to quantitatively distinguish the fast (direct effects of forcing on radiation, cloud, and land surface processes excluding the ocean response) and slow (oceanic processes) responses of the EASM to aerosol forcing. They suggested that an increased AA can weaken the EASM circulation and reduce precipitation over eastern China and the main reason for this was the fast response of atmospheric processes to AA forcing.

Remote aerosol also can affect the circulation and precipitation of EASM. Cowan and Cai (2011) used a coupled climate model to study the effects of Asian and non-Asian AA on the EASM in the twentieth century and indicated that non-Asian AA exacerbated the cooling over Europe and Asia relative to the surrounding oceans, and weakened the southerly wind, which suppresses the Asian summer monsoon precipitation. Wan et al. (2013) reported that, based on climate model simulations with prescribed SST, European black carbon (BC) aerosol enhanced tropospheric heating over the Eurasian Continent through a propagating wave train and horizontal air temperature advection, which can intensify the land–sea thermal contrast and therefore enhance the EASM. Mahmood and Li (2014) also suggested that the South Asian BC aerosol could decrease EASM precipitation in China through weakening the moist air transport toward East Asia from the Bay of Bengal and enhancing atmospheric stability in the Yangtze River basin. Based on the atmospheric component of the Met Office Hadley Centre Earth system model (HadGEM2-ES), Dong et al. (2015) found that anthropogenic sulfate from European emissions induced cooling and drying of the midtroposphere over Asia and reduced the land–sea thermal contrast, which led to high sea level pressure (SLP) anomalies over Asia and low SLP anomalies over the western North Pacific (WNP) and further weakened the EASM.

The previous studies that examined the effects of local and remote aerosols on the EASM have made a great contribution to our understanding of the response of East Asian climate to aerosols. The majority of model studies have suggested that the increase in AA over East Asia could weaken the EASM strength. However, few studies have explored the impacts of recent dipole changes in emissions of anthropogenic aerosols and their precursors over East Asia and South Asia on the EASM. In this study, we investigate the relative impacts of the decrease in AA emissions over East Asia and the increase in AA over South Asia between 2013 and 2017, based on the atmosphere model of the Community Earth System Model Version 2 (CESM2). The remainder of the paper is organized as follows. Section 2 describes the CESM2 model and experiments design. Section 3 analyzes the responses of EASM to the changing AA emissions from East and South Asia. Conclusions and discussions are given in section 4.

## 2. Model description and experiment design

In this study, the responses of EASM to AA emissions are examined using the Community Atmosphere Model version 6 (CAM6), which is the atmospheric component of CESM2 (Danabasoglu et al. 2020). Simulations are performed at a spatial resolution of 0.9° latitude × 1.25° longitude and 32 vertical layers from the surface to 3.6 hPa. In CAM6, aerosols are treated using the four-mode Modal Aerosol Model (X. Liu et al. 2016), which predicts the mass and number concentrations of major aerosol species including sulfate, BC, POM, secondary organic aerosol (SOA), mineral dust, and sea salt. Aerosols can interact with radiation, clouds and precipitation that are realistically represented in CAM6. Details of the CAM6/CESM2 can be found in Danabasoglu et al. (2020).

In this study, we use the Community Emissions Data System (CEDS) anthropogenic emissions of aerosols and precursors (Hoesly et al. 2018) that were developed for the Coupled Model Intercomparison Project Phase 6 (CMIP6) as the model input datasets. The anthropogenic emissions in China are replaced by Multiresolution Emission Inventory for China (MEIC) inventory, which has been shown to produce the consistent aerosol precursor loadings with satellite observations (F. Liu et al. 2016) and better capture the recent emission reductions in China (Wang et al. 2021). Biomass burning emissions are also from the standard CMIP6 datasets (van Marle et al. 2017).

Three 40-yr parallel equilibrium experiments, named BASE, EA17, and EASA17, are conducted with different AA emissions from East Asia and South Asia. The boundaries of East Asia and South Asia follow the source-receptor regions provided by the Hemispheric Transport of Air Pollution model experiment phase 2 (HTAP2). The AA emissions in both East Asia and South Asia are fixed at year 2013 levels in the BASE experiment, while East Asian emissions are changed to year 2017 levels in EA17 and AA emissions in 2017 are adopted for both East Asia and South Asia in EASA17. AA emissions in other regions of the world remain at year 2013 levels in all simulations. The seasonal cycle of emissions is considered in the simulations. The differences between the BASE experiment and other two experiments (EA17 and EASA17) are attributed to the effect of AA emissions reduction in East Asia and the dipole changes in the AA emissions over East Asia and South Asia, respectively. All experiments are driven by the climatological mean SST and SIC for the present-day climatology (average over 1995–2005). We note that only atmospheric rapid adjustments are considered in this study without the consideration of SST responses, and the land surface temperatures are allowed to respond to aerosol changes. The ozone, greenhouse gas forcing and biomass burning emissions are kept at year 2013 values

during simulations. Each experiment runs for 40 years and the averages of the last 35 years are used for analysis. Considering the uncertainty of the aerosol impacts on climate, the two-tailed Student's $t$ test with 90% confidence level is applied in the following analysis.

Effective radiative forcing (ERF) quantifies the net change in the energy budget of the Earth system after a perturbation, and includes the instantaneous forcing and rapid adjustments from the atmosphere and surface (Smith et al. 2020). The ERF in this study is diagnosed as the difference of net radiative flux between the perturbation experiments (EA17 and EASA17) and the control experiment (BASE). ERF due to aerosol–cloud interactions is decomposed based on Ghan (2013), defined as $\Delta(F_{\text{clean}} - F_{\text{clear,clean}})$, where $F_{\text{clean}}$ is the radiative flux neglecting the scattering and absorption of solar radiation by aerosols and $F_{\text{clear,clean}}$ is the radiative flux neglecting scattering and absorption by both clouds and aerosols. The difference between two simulations is represented by $\Delta$.

## 3. Results

### a. Model evaluation

Observed atmospheric circulation and precipitation during the EASM season are shown in Fig. 1a, which are from the NCEP–NCAR Reanalysis (Kalnay et al. 1996), ERA5 (Hersbach et al. 2020), and Global Precipitation Climatology Project (GPCP) datasets (Adler et al. 2018). Generally, the monsoon flow carrying moist air from the Bay of Bengal and Indochina Peninsula penetrates abruptly into the Yangtze River basin (26°–32°N, 105°–122.5°E) and extends to northern China (32°–42°N, 105°–122.5°E). During this period, the western Pacific subtropical high (WPSH) over the east of China mainland is important for the atmospheric conditions and precipitation in China. CAM6 reproduces well the climatological mean of the main features of EASM (Fig. 1b), although the precipitation in the Bay of Bengal and westerlies north of 40°N are overestimated. The spatial correlation coefficients of boreal summer (JJA) mean zonal and meridional winds at 850 hPa, SLP, and precipitation rate between observation and BASE experiment in 2013 over Asian regions are 0.87, 0.83, 0.87, and 0.70, respectively, suggesting that CAM6 has the ability to simulate the key features of EASM.

Changes in surface aerosol concentrations during 2013–17 simulated by CAM6 were evaluated in Gao et al. (2022). It was reported that the model could capture the changes in spatial distribution of aerosols concentrations in China, but strongly underestimated the magnitude of the concentration decreases by more than 50%. The low bias of the aerosol reduction could result in the underestimation of the responses in EASM, which is further discussed in the following section.

### b. Dipole changes in aerosol emissions, burden, and effective radiative forcing

The changes in JJA mean anthropogenic emissions of BC, POM, sulfur dioxide ($SO_2$), and SOA precursor gas (SOAG) between 2013 and 2017 are shown in Fig. 2 (changes over East Asia or South Asia are given in Fig. S1). Anthropogenic emissions of aerosols and precursor gases significantly decreased over eastern China from 2013 to 2017 due to the Air Pollution Prevention and Control Action Plan, but increased in the Indo-Gangetic Plain (IGP) region (25°–35°N, 70°–90°E), displaying a dipole pattern between East Asia and South Asia. The anthropogenic emissions over South India also decreased during 2013–17, which led to changes in burden of aerosols and could influence climate in Asia.

Changes in the spatial distribution of AA column burden are shown in Fig. 3 and corresponding percentage changes are shown in Fig. S2. Due to the reduction in AA emissions, the AA column burdens decreased significantly in East Asia in both EA17 and EASA17 experiments. Sulfate aerosol decreased most significantly, especially in northern China by 3–6 mg $m^{-2}$ (40%–60%), followed by POM (0.5–1 mg $m^{-2}$; 10%–30%), BC (0.2–0.5 mg $m^{-2}$; 20%–40%), and SOA (0.2–0.5 mg $m^{-2}$; 5%–10%). In South Asia, the changes in the column burden of AA between BASE and EASA17 are basically consistent with the changes in anthropogenic emissions. The largest increases in AA column burden are located over IGP regions. Relative to 2013, sulfate burden in 2017 was increased by 0.5–3 mg $m^{-2}$ (10%–20%), followed by POM (0.1–0.5 mg $m^{-2}$; 1%–10%) and BC (0.02–0.1 mg $m^{-2}$; 1%–10%), while SOA burden showed a weak decrease of less than 5% over South Asia.

As shown in Fig. 4a, the decrease in AA led to the positive aerosol ERF at the top of the atmosphere (TOA) over central-eastern China between 2013 and 2017, with a maximum change of 4–8 W $m^{-2}$. Averaged over central-eastern China (25°–40°N, 105°–122.5°), 2013–2017 changes in AA emissions induced a positive aerosol ERF of 1.59 (±0.97) W $m^{-2}$ (Table 1) relative to BASE. The decreases in AA emissions from East Asia also resulted in strong positive ERF of 2–8 W $m^{-2}$ over Japan and the surrounding ocean. The changes in ERF are primarily due to aerosol–cloud interactions in the case of AA emission reductions (Fig. S3). The decreases in aerosols transported to the western North Pacific caused the weakened negative ERF due to aerosol–cloud interactions, leading to an increase in radiation absorption by Earth. In addition, the decrease in BC aerosols suppressed the formation of low-level marine stratocumulus and increased high-level cloud amount over the western North Pacific (Fig. S4), as previously reported by Yang et al. (2019), which further intensified the positive aerosol ERF in EA17 relative to BASE. The reduced AA emissions in East Asia also led to stronger positive ERF at the surface than at TOA over central-eastern China, revealing the weakened atmospheric absorption by absorbing aerosols related to the emission reductions (Fig. S5).

Due to the increases in AA emissions over the IGP region, the negative ERF of AA was strengthened by 2–8 W $m^{-2}$ during 2013–17, while positive ERF was located over South India (Fig. 4b) due to the decrease in low-level cloud (Fig. S4b) during this time period. Interestingly, the positive ERF over eastern China due to the decreases in AA emissions over East Asia was strengthened by the increases in emissions over South Asia. The regional averaged ERF over central-eastern China increased from 1.59 (±0.97) W $m^{-2}$ in EA17 to 3.39 (±0.89) W $m^{-2}$ in EASA17, relative to BASE experiment, likely due to feedbacks through changes in atmospheric

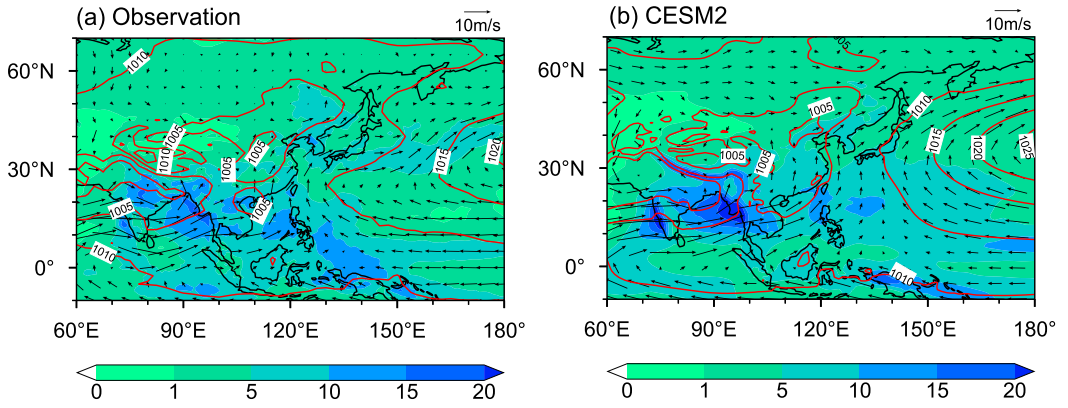


FIG. 1. June–August (JJA) mean 850-hPa winds (vectors; m $s^{-1}$), sea level pressure (contours; hPa), and precipitation (shaded colors; mm $day^{-1}$) in 2013 derived (a) from NCEP–NCAR Reanalysis (for sea level pressure), ERA5 (for winds), and Global Precipitation Climatology Project (GPCP) dataset (for precipitation) and (b) from the BASE experiment of CAM6.

circulation and clouds associated with the increases in AA emissions from South Asia, which is further examined below.

### c. *Change in East Asian climate due to the dipole changes in emissions*

The perturbation of radiation flux associated with the dipole changes in AA emissions during 2013–17 can further change the surface air temperature, as shown in Fig. 5. Due to the reductions in AA emissions from East Asia, surface air temperature increased between 30° and 45°N over China and the downwind western North Pacific, with the maximum temperature increase of 0.2°–0.4°C (Fig. 5a). Temperature also decreased in southwestern China and increased in Southeast Asia, likely resulting from the increase/decrease in midlevel

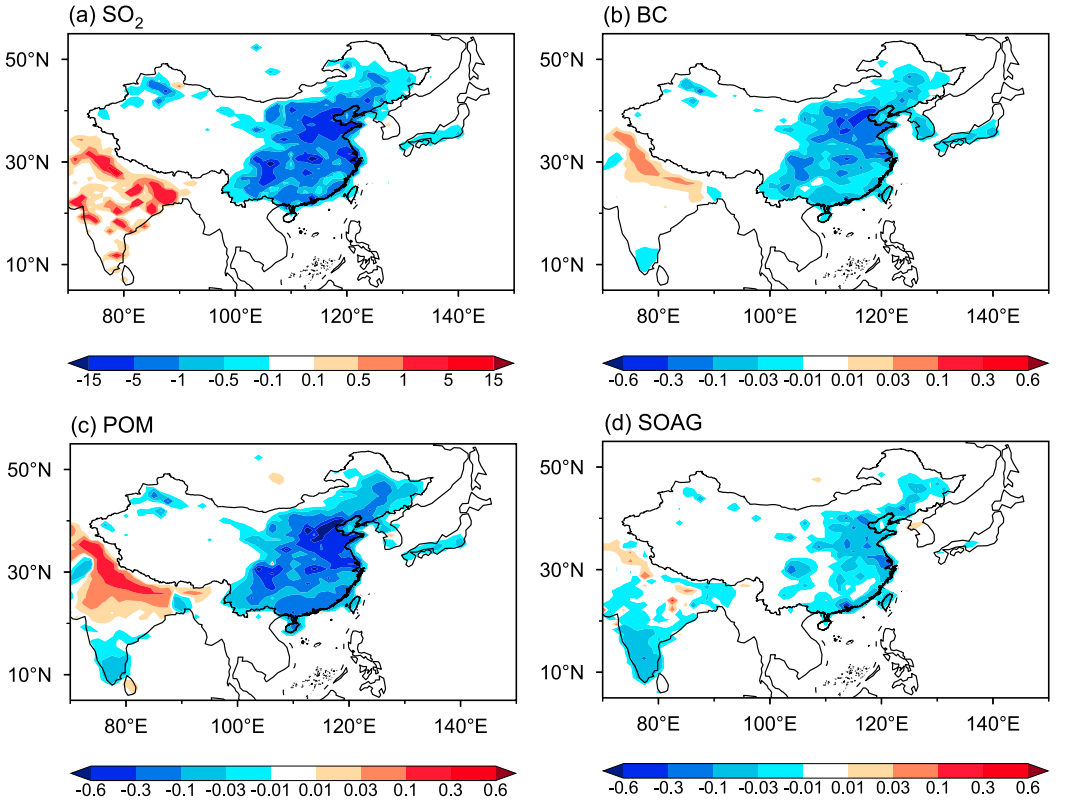


FIG. 2. Changes in June–August (JJA) mean anthropogenic emissions of (a) $SO_2$, (b) BC, (c) POM, and (d) SOAG (g $m^{-2}$ $yr^{-1}$) between 2013 and 2017.

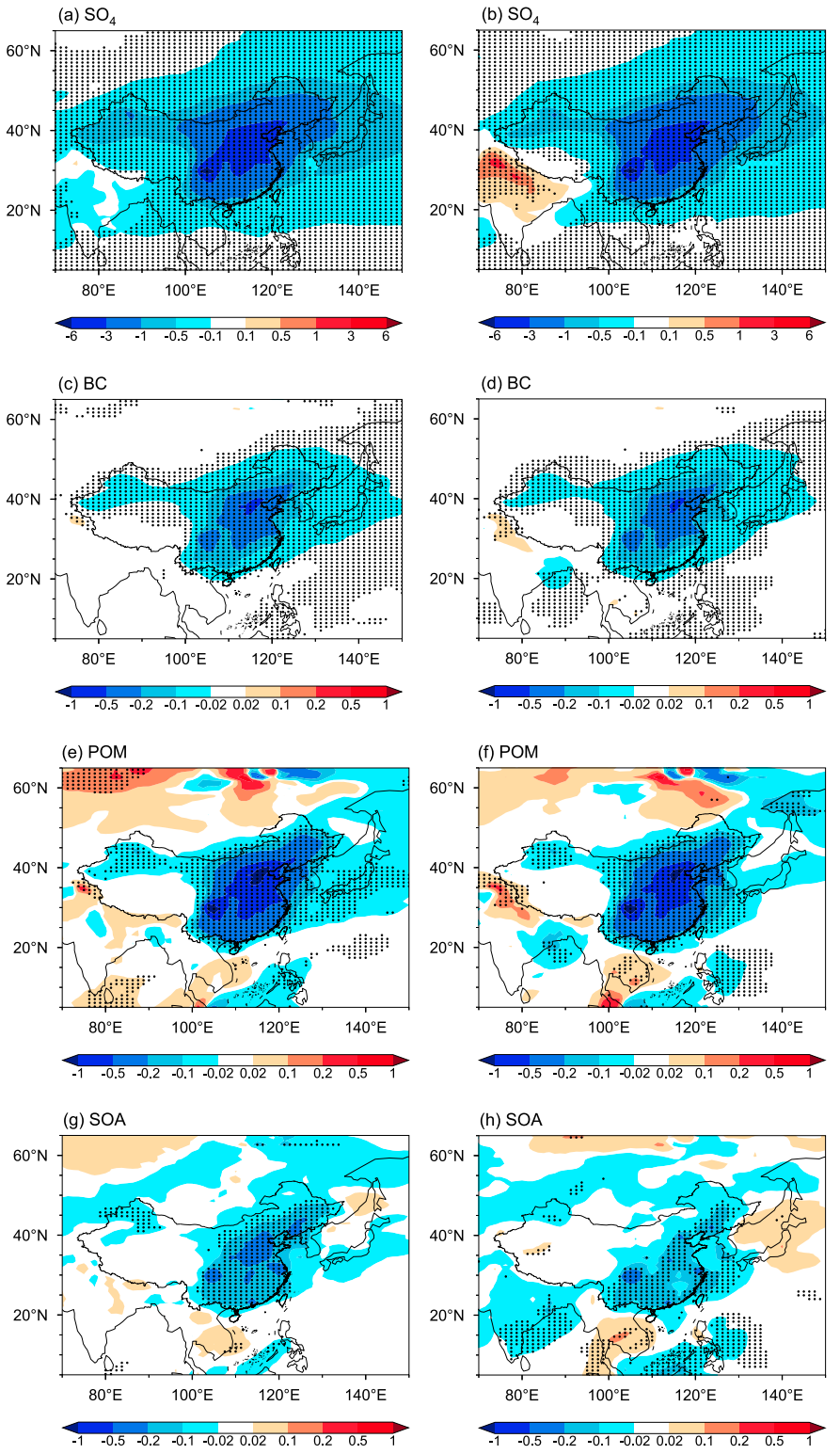


FIG. 3. Changes in JJA mean column burden of (a),(b) sulfate; (c),(d) BC; (e),(f) POM; and (g),(h) SOA (mg $m^{-2}$) between BASE and EA17 (EA17–BASE) and between BASE and EASA17 (EASA17–BASE), respectively. The dotted areas indicate statistical significance with 90% confidence based on a two-tailed Student's *t* test.

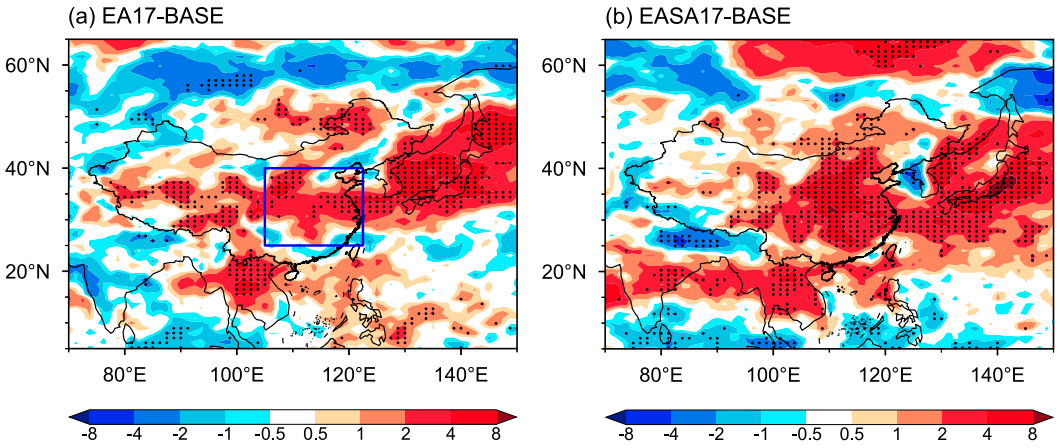


FIG. 4. Changes in JJA mean aerosol ERF (W $m^{-2}$) (a) between BASE and EA17 (EA17 − BASE) and (b) between BASE and EASA17 (EASA17 − BASE). The dotted areas indicate statistical significance with 90% confidence based on a two-tailed Student's $t$ test. The blue box in (a) marks central-eastern China (25°–40°N, 105°–122.5°E).

cloud (Fig. S4c) caused by the aerosol-induced changes in atmospheric circulation. When considering both the decrease in AA emissions in East Asia and the increase in AA emissions in South Asia, surface temperature shows a weak decrease over the IGP region, but the temperature increase in central-eastern China was stronger, with the maximum temperature increase of 0.4°–0.6°C (Fig. 5b). A weak cooling appears over the northwestern Pacific, which may be related to the downdraft of cold air due to the strengthened WPSH (Yang et al. 2022). Averaged over central-eastern China, the surface air temperature anomaly induced by the reductions in AA emissions from East Asia was doubled, from 0.09 (±0.07)° to 0.20 (±0.08)°C (Table 1), with the simultaneous increase in AA emissions from South Asia.

The enhanced summer warming over central-eastern China in EASA17, compared to EA17, is the result of the intensified and westward shift of the WPSH that can be linked to the increase in BC aerosol in South Asia. The enhanced warming over land caused by the reductions in East Asian emissions of AA intensified the land–sea thermal contrast between eastern China and the western North Pacific, resulting in a strengthened WPSH (Fig. 6a). The increases in BC aerosols in South Asia led to anomalous atmospheric heating over 70°–80°E (Fig. S6a), which produced an anomalous ascending flow over this region (Fig. S6b). The anomalous ascend over South Asia enhanced the anomalous subsidence over 110°–130°E, causing the intensified and westward shift of the WPSH (Fig. S7a), adding to the effect of reductions in AA emissions from East Asia (Fig. 6b). The enhanced intensity and westward shift of WPSH can increase the atmospheric stability and suppress the cloud formation (Fig. S4), leading to a warmer climate over central-eastern China in EASA17 than in EA17.

The most significant feature of precipitation changes due to the reductions in AA emissions from East Asia was an enhanced summer rainfall over central-eastern China (Fig. 7a). It was related to the anomalous southerly winds along the west edge of the strengthened WPSH (Fig. 6a), which brought warm and moist air from South China Sea to southern China (18°–32°N, 105°–122.5°E), and increased cloud amount there (Figs. S4a,c,e). Averaged over central-eastern China, the JJA precipitation was increased by 0.32 (±0.16) mm $day^{-1}$ in EA17 compared to BASE experiment (Table 1). The impact of the dipole pattern of the Asian AA emission changes on EASM precipitation is complex (Fig. 7b). Although precipitation in central-eastern China increased due to the anomalous moisture transport associated with the East Asian emission reductions, the westward shift of WPSH due to the South Asian emission (Fig. S7a) increased the atmospheric stability and tended to decrease precipitation over central eastern China and the western North Pacific (Fig. S7b). This can be further confirmed by the anomalous downdraft over 20°–40°N in central-eastern China (Fig. S8b). The dipole changes in emissions caused increased precipitation in the northeast (the Korean peninsula) and southwest (Yunnan–Myanmar border), but deficits in the central and southeast regions, with an insignificant regional averaged change of −0.07 (±0.16) mm $day^{-1}$ in EASA17 compared to BASE experiment.

TABLE 1. Regional mean differences in effective radiative forcing (ERF), temperature at 2 m (T2m), meridional wind at 850 hPa (V850), and precipitation rate between EA17 and BASE and between EA17 and EASA17 over central-eastern China (25°–40°N, 105°–122.5°E) in JJA. Values in parentheses are 1$\sigma$ for the 35 seasonal means.

| Expt | ERF (W $m^{-2}$) | T2m (°C) | V850 (m $s^{-1}$) | Precipitation (mm $day^{-1}$) |
|---|---|---|---|---|
| EA17-BASE | +1.59 (±0.97) | +0.09 (±0.07) | +0.25 (±0.22) | +0.32 (±0.16) |
| EASA17-BASE | +3.39 (±0.89) | +0.20 (±0.08) | +0.39 (±0.21) | –0.07 (±0.16) |

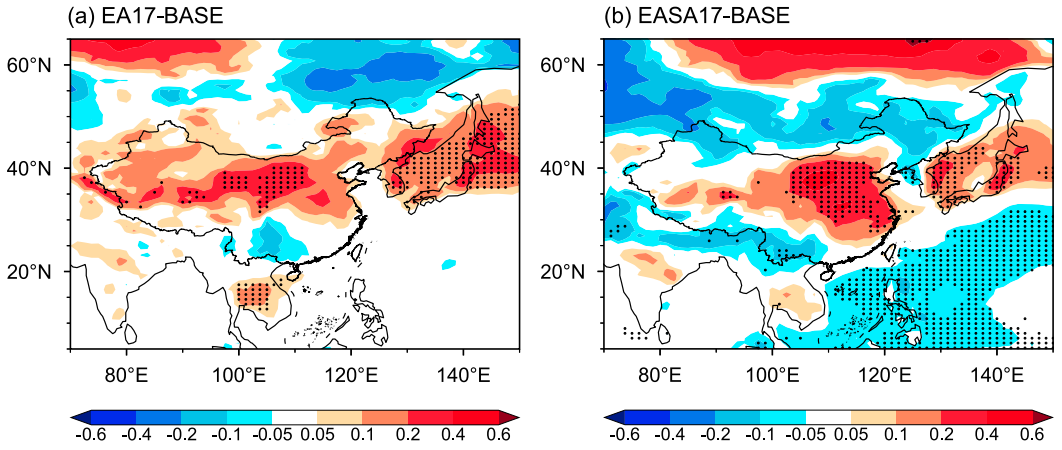


FIG. 5. Changes in JJA mean surface air temperature (°C) (a) between BASE and EA17 (EA17 − BASE) and (b) between BASE and EASA17 (EASA17 − BASE). The dotted areas indicate statistical significance with 90% confidence based on a two-tailed Student's *t* test.

The changes in JJA mean SLP, 850-hPa winds, and precipitation between 2013 (average of 2011–15 to remove the internal variability in observations) and 2017 (average of 2015–19) from observations are also shown in Fig. 8 (and Fig. S9) for reference. During 2013–17, observations also show the intensified and westward shift of WPSH and the increases in the southwesterly winds over southern China, similar to the modeling results, indicating that the recent change in EASM circulation can be largely explained by the dipole changes in AA emissions over East Asia and South Asia. The observed EASM precipitation increased over central-eastern China and decreased over the western North Pacific in 2017 compared to 2013, similar to the effects of East Asian emission changes in model. Note that, however, the changes in atmospheric circulation and precipitation of EASM are affected by many other factors than aerosols, such as climate change, changes in SST, and modes of internal variability. A few differences are also shown in observations, such as the increase in precipitation over central China and the less significant enhancement of WPSH in observations, which cannot be explained by the changes in AA alone. In addition, the model underestimated the aerosol decrease in eastern China during 2013–17 (Gao et al. 2022), which can lead to a low bias in the simulated response of EASM precipitation to AA emission reductions from East Asia.

### d. *Quantifying the change in EASM intensity*

As examined above, the decreases in AA emissions from East Asia intensified WPSH and the increases in AA emissions from South Asia further led to the westward shift of WPSH, enhancing the intensity of EASM (Wang et al. 2013). However, to what extent the dipole changes in AA emissions over East Asia and South Asia influence the EASM needs quantitative analysis.

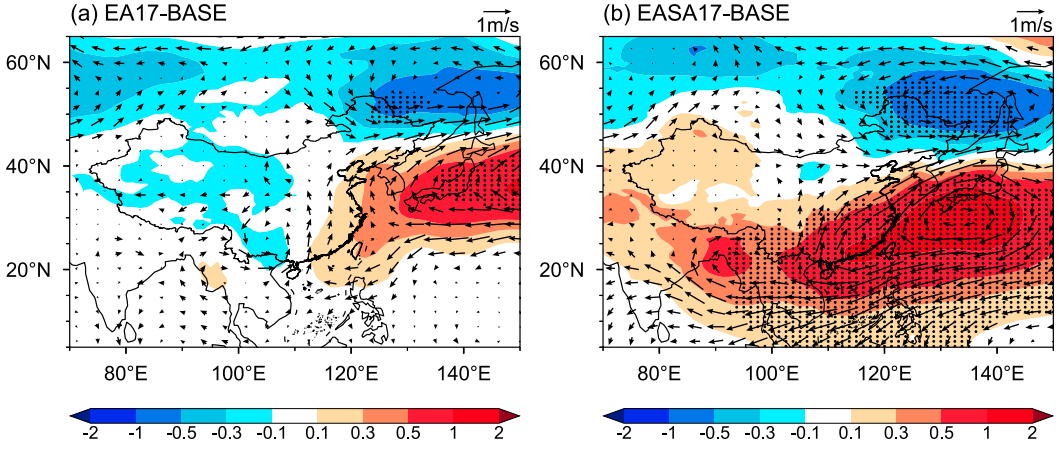


FIG. 6. Changes in JJA mean sea level pressure (colors; hPa) and 850-hPa winds (vectors; m $s^{-1}$) (a) between BASE and EA17 (EA17 − BASE) and (b) between BASE and EASA17 (EASA17 − BASE). The dotted areas indicate statistical significance with 90% confidence based on a two-tailed Student's *t* test.

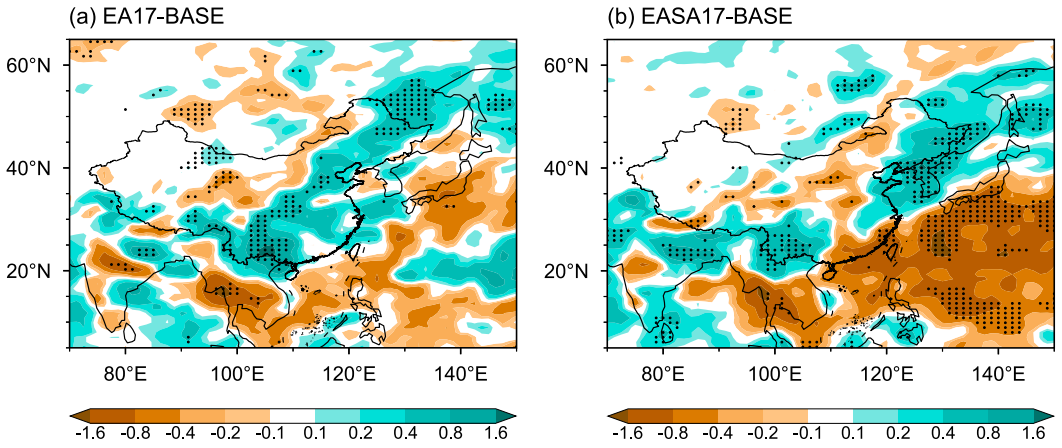


FIG. 7. Changes in JJA mean precipitation (mm day$^{-1}$) (a) between BASE and EA17 (EA17 − BASE) and (b) between BASE and EASA17 (EASA17 − BASE). The dotted areas indicate statistical significance with 90% confidence based on a two-tailed Student's *t* test.

In this study, three indices (i.e., $I_{Sun}$, $I_{Lau}$, and $I_{Wu}$) that include different features of east–west and north–south thermal contrast (Sun et al. 2002), north–south shear vorticity (Lau et al. 2000) and southwest monsoon (Wu and Ni 1997), respectively, are employed to quantify the intensity of EASM, as shown in Table S1. The three indices are individually calculated using surface air temperature, zonal winds at 200 hPa, and meridional winds at 850 hPa, respectively. Using three different indices can give a more robust result than that from any individual index.

Compared to the BASE experiment, the EASM intensity in EA17 is increased by 4.1%, 0.6%, and 4.5%, respectively, for $I_{Sun}$, $I_{Lau}$, and $I_{Wu}$, indicating that the reductions in AA emissions from East Asia during 2013–17 enhanced the EASM strength by less than 5%. With the effects of increases in AA emissions from South Asia superimposed, the increases are enlarged to 14.9%, 9.4%, and 5.0% in the EASA17 experiment. It suggests that, besides the decreases in East Asian emissions, the increases in South Asian emissions of AA have a crucial impact on the intensified EASM strength. The dipole changes in AA emissions over East Asia and South Asia together enhanced the EASM by 5%–15% during 2013–17.

## 4. Conclusions and discussion

China implemented the air pollution prevention and control action plan in 2013, which significantly reduced the emissions of anthropogenic aerosols (AA) and precursors. Meanwhile, AA emissions in South Asia have been continually increasing, which formed a dipole pattern of changes in AA emissions between South Asia and East Asia during 2013–17. In this study, the response of EASM to the dipole changes in AA emissions are investigated based on CESM2-CAM6 emissions sensitivity simulations.

Along with the decreases in East Asian AA emissions, a positive aerosol ERF of 1.59 (±0.97) W m$^{-2}$ relative to

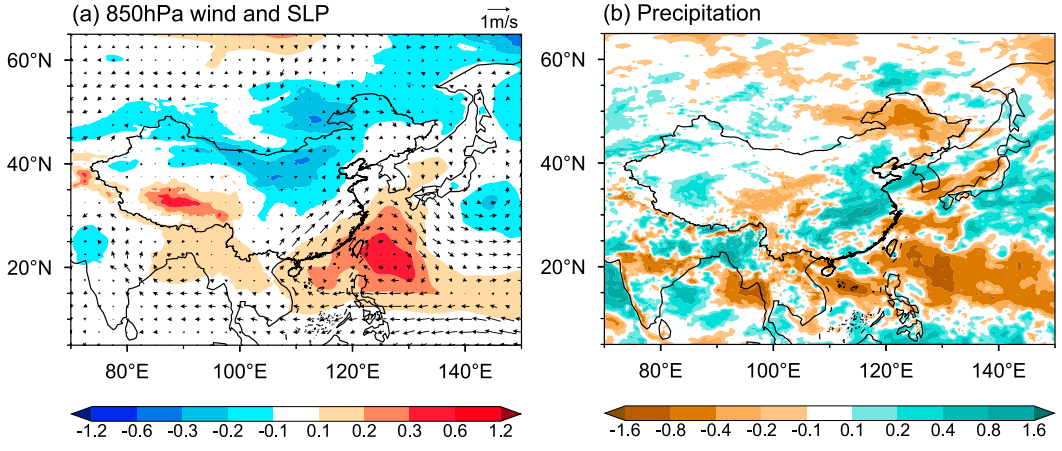


FIG. 8. Changes in JJA mean (a) sea level pressure (colors; hPa) and 850-hPa winds (vectors; m s$^{-1}$) and (b) precipitation rate (mm day$^{-1}$) between 2013 (represented by the average of 2011–15) and 2017 (represented by the average of 2015–19) derived from ERA5.

BASE appears in central-eastern China (25°–40°N, 105°–122.5°E) in summer, resulting in a 0.09 (±0.07)°C warming during 2013–17. The anomalous warming over land intensified the land–sea thermal contrast between eastern China and the western North Pacific, which resulted in a strengthened WPSH and an increase in summer precipitation by 0.32 (±0.16) mm day$^{-1}$ over central-eastern China. When considering both the AA reductions in East Asia and increases in South Asia, the ERF relative to BASE is increased to 3.39 (±0.89) W m$^{-2}$, along with an enhanced warming of 0.20 (±0.08)°C over central-eastern China, which is the result of westward shift of the strengthened WPSH linked to the increase in BC aerosol in South Asia. The combined effect of the stabilized air and moisture transport associated with the WPSH led to a −0.07 (±0.16) mm day$^{-1}$ precipitation change related to the changes in Asian AA emissions during 2013–17.

Based on the quantitative estimation of multiple EASM indices, the reductions in AA emissions from East Asia during 2013–17 are found to enhance the EASM strength by less than 5%, while the dipole changes in AA emissions over East Asia and South Asia together enhanced the EASM by 5%–15% during 2013–17, revealing an important role of South Asian AA emissions in changing the East Asian climate. However, we also note that although the dipole pattern of changes in AA emissions over Asia leads to stronger land–sea thermal contrast and circulations changes in comparison with responses to AA reductions over East Asia alone, precipitation does not show a stronger response to the dipole changes in AA emissions over East Asia and South Asia due to precipitation suppression caused by South Asian AA emissions.

This study focuses on the EASM response to Asian emissions dipole changes in JJA. However, change in AA in pre- and post-monsoon seasons may also influence the climate in East Asia (Ramachandran et al. 2020). As shown in Fig. S10, the responses of circulation and precipitation over central-eastern China to changes in East Asian AA emissions reach their maximums in JJA, while temperature response decreases from April to September. With both changes in AA emissions over East Asia and South Asia included, the climate responses are strongest in July, while the South Asian emissions enhance precipitation in September.

Note that, Gao et al. (2022) used the same model to investigate the climatic impacts of changes in aerosols and ozone due to China's recent clean air actions by perturbing aerosol emissions and ozone concentrations over China. They found that the increase in ozone can intensify the warming caused by the aerosol reductions in China. Our study answers how and to what extent the spatial dipole pattern in Asian aerosol changes could influence EASM through changing AA emissions over East Asia and South Asia, which has the different scientific focus and experimental design compared to Gao et al. (2022).

Our study also has some limitations and uncertainties. First, although the atmospheric rapid adjustments were previously reported as the main process of EASM response to AA (Mu and Wang 2020), the dipole pattern of AA emissions can also influence the EASM through slow oceanic processes and air–sea interactions, which deserves further investigation by performing simulations with the consideration of SST responses. Second, the current version of CESM2-CAM6 does not treat nitrate and ammonium aerosols; however, their changes in 2013–17 could also affect the EASM, although slight changes were found in nitrate concentration in Beijing during this time (Zhang et al. 2020). Third, the model strongly underestimates the magnitude of regional surface aerosol concentrations (Gao et al. 2022; Ren et al. 2021; Zeng et al. 2021; Yang et al. 2017a,c) and, therefore, the reduction in AA burden in China is also likely to be underestimated, which may lead to a low bias of the response of EASM to the changes in AA emissions from East Asia. Last but not the least, the conclusions here are based on the CESM2-CAM6 simulations, and therefore more comprehensive study is required in the future to conclusively answer the question as to what extent the dipole influences the EASM.

*Acknowledgments.* This study was supported by the National Natural Science Foundation of China (Grant 41975159), the National Key Research and Development Program of China (Grants 2019YFA0606800 and 2020YFA0607803), Jiangsu Science Fund for Distinguished Young Scholars (Grant BK20211541), and Jiangsu Science Fund for Carbon Neutrality (Grant BK20220031). H.W. acknowledges support from the U.S. Department of Energy (DOE), Office of Science, Office of Biological and Environmental Research (BER), as part of the Earth and Environmental System Modeling program. The Pacific Northwest National Laboratory (PNNL) is operated for DOE by the Battelle Memorial Institute under Contract DE-AC05-76RLO1830.

*Data availability statement.* Observed sea level pressure data in section 3a are available at https://psl.noaa.gov/data/gridded/data.ncep.reanalysis.html (last access: October 2022). Observed 850-hPa winds in sections 3a and 3c are available at https://cds.climate.copernicus.eu/cdsapp#!/dataset/reanalysis-era5-pressure-levels-monthly-means?tab=form (last access: October 2022). Observed precipitation rate data in section 3a are available at https://www.ncei.noaa.gov/data/global-precipitation-climatology-project-gpcp-daily/access/2013 (last access: October 2022). Observed sea level pressure and precipitation rate in section 3c are available at https://cds.climate.copernicus.eu/cdsapp#!/dataset/reanalysis-era5-single-levels-monthly-means?tab=form (last access: October 2022). The CESM2 model data are available at https://escomp.github.io/CESM/versions/cesm2.1/html/downloading_cesm.html (last access: October 2022). The MEIC inventory can be downloaded at http://meicmodel.org/?page_id=541&lang=en (last access: October 2022).

## REFERENCES

Adler, R. F., and Coauthors, 2018: The Global Precipitation Climatology Project (GPCP) monthly analysis (new version 2.3) and a review of 2017 global precipitation. *Atmosphere*, **9**, 138, https://doi.org/10.3390/atmos9040138.

Bell, M. L., and D. L. Davis, 2001: Reassessment of the lethal London fog of 1952: Novel indicators of acute and chronic consequences of acute exposure to air pollution. *Environ.*

*Health Perspect.*, **109**, 389–394, https://doi.org/10.1289/ehp.01109s3389.

Cohen, A. J., and Coauthors, 2017: Estimates and 25-year trends of the global burden of disease attributable to ambient air pollution: An analysis of data from the Global Burden of Diseases Study 2015. *Lancet*, **389**, 1907–1918, https://doi.org/10.1016/S0140-6736(17)30505-6.

Cowan, T., and W. Cai, 2011: The impact of Asian and non-Asian anthropogenic aerosols on 20th century Asian summer monsoon. *Geophys. Res. Lett.*, **38**, L11703, https://doi.org/10.1029/2011GL047268.

Danabasoglu, G., and Coauthors, 2020: The Community Earth System Model version 2 (CESM2). *J. Adv. Model Earth Syst.*, **12**, e2019MS001916, https://doi.org/10.1029/2019MS001916.

Ding, Y.-H., and J. C. L. Chan, 2005: The East Asian summer monsoon: An overview. *Meteor. Atmos. Phys.*, **89**, 117–142, https://doi.org/10.1007/s00703-005-0125-z.

Dong, B., R. T. Sutton, E. J. Highwood, and L. J. Wilcox, 2015: Preferred response of the East Asian summer monsoon to local and non-local anthropogenic sulphur dioxide emissions. *Climate Dyn.*, **46**, 1733–1751, https://doi.org/10.1007/s00382-015-2671-5.

——, L. J. Wilcox, E. J. Highwood, and R. T. Sutton, 2019: Impacts of recent decadal changes in Asian aerosols on the East Asian summer monsoon: Roles of aerosol–radiation and aerosol–cloud interactions. *Climate Dyn.*, **53**, 3235–3256, https://doi.org/10.1007/s00382-019-04698-0.

Gao, J., and Coauthors, 2022: Fast climate responses to emission reductions in aerosol and ozone precursors in China during 2013–2017. *Atmos. Chem. Phys.*, **22**, 7131–7142, https://doi.org/10.5194/acp-22-7131-2022.

Ghan, S. J., 2013: Technical note: Estimating aerosol effects on cloud radiative forcing. *Atmos. Chem. Phys.*, **13**, 9971–9974, https://doi.org/10.5194/acp-13-9971-2013.

Hersbach, H., and Coauthors, 2020: The ERA5 global renanlysis. *Quart. J. Roy. Meteor. Soc.*, **146**, 1999–2049, https://doi.org/10.1002/qj.3803.

Hoesly, R. M., and Coauthors, 2018: Historical (1750–2014) anthropogenic emissions of reactive gases and aerosols from the Community Emissions Data System (CEDS). *Geosci. Model Dev.*, **11**, 369–408, https://doi.org/10.5194/gmd-11-369-2018.

Jiang, Y., X. Liu, X.-Q. Yang, and M. Wang, 2013: A numerical study of the effect of different aerosol types on East Asian summer clouds and precipitation. *Atmos. Environ.*, **70**, 51–63, https://doi.org/10.1016/j.atmosenv.2012.12.039.

Kalnay, E., and Coauthors, 1996: The NCEP/NCAR 40-Year Reanalysis Project. *Bull. Amer. Meteor. Soc.*, **77**, 437–472, https://doi.org/10.1175/1520-0477(1996)077<0437:TNYRP>2.0.CO;2.

Lau, K.-M., K.-M. Kim, and S. Yang, 2000: Dynamical and boundary forcing characteristics of regional components of the Asia summer monsoon. *J. Climate*, **13**, 2461–2482, https://doi.org/10.1175/1520-0442(2000)013<2461:DABFCO>2.0.CO;2.

——, and Coauthors, 2008: The Joint Aerosol–Monsoon Experiment: A new challenge for monsoon climate research. *Bull. Amer. Meteor. Soc.*, **89**, 369–384, https://doi.org/10.1175/BAMS-89-3-369.

Lei, Y., B. Hoskins, and J. Slingo, 2011: Exploring the interplay between natural decadal variability and anthropogenic climate change in summer rainfall over China. Part I: Observational evidence. *J. Climate*, **24**, 4584–4599, https://doi.org/10.1175/2010JCLI3794.1.

Li, Z., and Coauthors, 2016: Aerosol and monsoon climate interactions over Asia. *Rev. Geophys.*, **54**, 866–929, https://doi.org/10.1002/2015RG000500.

Liu, F., S. Beirle, Q. Zhang, S. Dörner, K. He, and T. Wagner, 2016: $NO_x$ lifetimes and emissions of cities and power plants in polluted background estimated by satellite observations. *Atmos. Chem. Phys.*, **16**, 5283–5298, https://doi.org/10.5194/acp-16-5283-2016.

Liu, X., P.-L. Ma, H. Wang, S. Tilmes, B. Singh, R. C. Easter, S. J. Ghan, and P. J. Rasch, 2016: Description and evaluation of a new four-mode version of the Modal Aerosol Module (MAM4) within version 5.3 of the Community Atmosphere Model. *Geosci. Model Dev.*, **9**, 505–522, https://doi.org/10.5194/gmd-9-505-2016.

Mahmood, R., and S. Li, 2014: Remote influence of South Asian black carbon aerosol on East Asian summer climate. *Int. J. Climatol.*, **34**, 36–48, https://doi.org/10.1002/joc.3664.

Mu, J., and Z. Wang, 2020: Responses of the East Asian summer monsoon to aerosol forcing in CMIP5 models: The role of upper-tropospheric temperature change. *Int. J. Climatol.*, **41**, 1555–1570, https://doi.org/10.1002/joc.6887.

Ramachandran, S., M. Rupakheti, and M. G. Lawrence, 2020: Black carbon dominates the aerosol absorption over the Indo-Gangetic Plain and the Himalayan foothills. *Environ. Int.*, **142**, 105814, https://doi.org/10.1016/j.envint.2020.105814.

——, ——, and R. Cherian, 2022: Insights into recent aerosol trends over Asia from observations and CMIP6 simulations. *Sci. Total Environ.*, **807**, 150756, https://doi.org/10.1016/j.scitotenv.2021.150756.

Ren, L., Y. Yang, H. Wang, P. Wang, L. Chen, J. Zhu, and H. Liao, 2021: Aerosol transport pathways and source attribution in China during the COVID-19 outbreak. *Atmos. Chem. Phys.*, **21**, 15 431–15 445, https://doi.org/10.5194/acp-21-15431-2021.

Samset, B. H., M. T. Lund, M. Bollasina, G. Myhre, and L. Wilcox, 2019: Emerging Asian aerosol patterns. *Nat. Geosci.*, **12**, 582–584, https://doi.org/10.1038/s41561-019-0424-5.

Smith, C. J., and Coauthors, 2020: Effective radiative forcing and adjustments in CMIP6 models. *Atmos. Chem. Phys.*, **20**, 9591–9618, https://doi.org/10.5194/acp-20-9591-2020.

Sun, X., L. Chen, and J. He, 2002: Index of land-sea thermal difference and its relation to interannual variation of summer circulation and rainfall over East Asia (in Chinese). *Acta Meteor. Sin.*, **60**, 164–172, https://doi.org/10.11676/qxxb2002.020.

Tian, F., B. Dong, J. Robson, and R. Sutton, 2018: Forced decadal changes in the East Asian summer monsoon: The roles of greenhouse gases and anthropogenic aerosols. *Climate Dyn.*, **51**, 3699–3715, https://doi.org/10.1007/s00382-018-4105-7.

van Marle, M. J. E., and Coauthors, 2017:: Historic global biomass burning emissions for CMIP6 (BB4CMIP) based on merging satellite observations with proxies and fire models (1750–2015). *Geosci. Model Dev.*, **10**, 3329–3357, https://doi.org/10.5194/gmd-10-3329-2017.

Wan, J.-H., R. Mahmood, and S. Li, 2013: Impact of European black carbon on East Asian summer climate. *Atmos. Oceanic Sci. Lett.*, **6**, 375–380, https://doi.org/10.3878/j.issn.1674-2834.13.0037.

Wang, B., B. Xiang, and J.-Y. Lee, 2013: Subtropical high predictability establishes a promising way for monsoon and tropical storm predictions. *Proc. Natl. Acad. Sci. USA*, **110**, 2718–2722, https://doi.org/10.1073/pnas.1214626110.

Wang, Z., and Coauthors, 2021: Incorrect Asian aerosols affecting the attribution and projection of regional climate change in

CMIP6 models. *npj Climate Atmos. Sci.*, **4**, 2, https://doi.org/10.1038/s41612-020-00159-2.

Wu, A., and Y. Ni, 1997: The influence of Tibetan Plateau on the interannual variability of Asian monsoon. *Adv. Atmos. Sci.*, **14**, 491–504, https://doi.org/10.1007/s00376-997-0067-0.

Xie, X., H. Wang, X. Liu, J. Li, Z. Wang, and Y. Liu, 2016: Distinct effects of anthropogenic aerosols on the East Asian summer monsoon between multidecadal strong and weak monsoon stages. *J. Geophys. Res. Atmos.*, **121**, 7026–7040, https://doi.org/10.1002/2015JD024228.

Yang, Y., H. Wang, S. J. Smith, P.-L. Ma, and P. J. Rasch, 2017a: Source attribution of black carbon and its direct radiative forcing in China. *Atmos. Chem. Phys.*, **17**, 4319–4336, https://doi.org/10.5194/acp-17-4319-2017.

——, L. M. Russell, S. Lou, H. Liao, J. Guo, Y. Liu, B. Singh, and S. J. Ghan, 2017b: Dust-wind interactions can intensify aerosol pollution over eastern China. *Nat. Commun.*, **8**, 15333, https://doi.org/10.1038/ncomms15333.

——, and Coauthors, 2017c: Global source attribution of sulfate concentration and direct and indirect radiative forcing. *Atmos. Chem. Phys.*, **17**, 8903–8922, https://doi.org/10.5194/acp-17-8903-2017.

——, S. J. Smith, H. Wang, C. M. Mills, and P. J. Rasch, 2019: Variability, timescales, and nonlinearity in climate responses to black carbon emissions. *Atmos. Chem. Phys.*, **19**, 2405–2420, https://doi.org/10.5194/acp-19-2405-2019.

——, L. Ren, H. Li, H. Wang, P. Wang, L. Chen, X. Yue, and L. Hong, 2020: Fast climate responses to aerosol emission reductions during the COVID-19 pandemic. *Geophys. Res. Lett.*, **47**, e2020GL089788, https://doi.org/10.1029/2020GL089788.

——, and Coauthors, 2022: Abrupt emissions reductions during COVID-19 contributed to record summer rainfall in China. *Nat. Commun.*, **13**, 959, https://doi.org/10.1038/s41467-022-28537-9.

Yu, H., and Coauthors, 2013: A multimodel assessment of the influence of regional anthropogenic emission reductions on aerosol direct radiative forcing and the role of intercontinental transport. *J. Geophys. Res. Atmos.*, **118**, 700–720, https://doi.org/10.1029/2012JD018148.

Zeng, L., and Coauthors, 2021: Intensified modulation of winter aerosol pollution in China by El Niño with short duration. *Atmos. Chem. Phys.*, **21**, 10745–10761, https://doi.org/10.5194/acp-21-10745-2021.

Zhang, H., and Coauthors, 2011: Simulation of direct radiative forcing of aerosols and their effects on East Asian climate using an interactive AGCM-aerosol coupled system. *Climate Dyn.*, **38**, 1675–1693, https://doi.org/10.1007/s00382-011-1131-0.

Zhang, X. Y., Y. Q. Wang, T. Niu, X. C. Zhang, S. L. Gong, Y. M. Zhang, and J. Y. Sun, 2012: Atmospheric aerosol compositions in China: Spatial/temporal variability, chemical signature, regional haze distribution and comparisons with global aerosols. *Atmos. Chem. Phys.*, **12**, 779–799, https://doi.org/10.5194/acp-12-779-2012.

Zhang, Z., H. Guan, L. Luo, N. Zheng, and H. Xiao, 2020: Response of fine aerosol nitrate chemistry to clean air action in winter Beijing: Insights from the oxygen isotope signatures. *Sci. Total Environ.*, **746**, 141210, https://doi.org/10.1016/j.scitotenv.2020.141210.

Zheng, B., and Coauthors, 2018: Trends in China's anthropogenic emissions since 2010 as the consequence of clean air actions. *Atmos. Chem. Phys.*, **18**, 14095–14111, https://doi.org/10.5194/acp-18-14095-2018.